Characterization of Soot Precursor Emissions in Fuel Rich Premixed Flow Reactors

A Thesis

Presented to

the Faculty of the School of Engineering and Applied Science

University of Virginia

In Partial Fulfillment

of the Requirements for the Degree of

Master of Science in Mechanical and Aerospace Engineering

by

John N. Greenwood

May 2012

APPROVAL SHEET

This thesis is submitted in partial fulfillment of the requirements for the degree of

Master of Science in Mechanical and Aerospace Engineering

_____

John Greenwood, Author

This thesis has been read and approved by the Examining Committee:

_____

Harsha K. Chelliah, Thesis Advisor

_____

Houston G. Wood, Committee Chair

_____

Roland H. Krauss, Committee Member

Accepted for the School of Engineering and Applied Science:

_____

Dean, School of Engineering and Applied Science

May 2012

Abstract

Particulate emission from gas turbine engines is known to have a detrimental effect on human health. In anticipation of more stringent environmental regulations, methods of mitigation of nano-sized soot particle emission have been a key focus of gas turbine manufacturers. A better understanding of the conditions that lead to soot particle formation will assist development of new strategies to reduce such emissions and is the focus of this work.

Sooting conditions can be studied using premixed flow reactors, which are a commonly used laboratory apparatus to experimentally examine the evolution of combustion products. Fuel, oxidizer, and diluents are thoroughly mixed before entering a heated length of tube where they react. In order to adequately explore sooting regimes, it is desirable for the reactor to be able to rapidly heat the mixture to a target temperature (950 to 1150 K) for a range of fluid velocities or residence times (up to 300 msec), pressures (up to 10 atm), and composition (equivalence ratios greater than 1.8). This work analyzes the ability of a new microflow tube reactor to achieve target operating conditions and the subsequent oxidation process.

Specifically, increases in fluid velocity and pressure required high heating rates that place extreme thermal burdens on the current heater hardware. Thus, the experiments became increasingly difficult for low residence times resulting in an undesirably long transition regime. This study further illustrates that the high wall temperatures necessary at extreme conditions introduce severe radial temperature gradients which cause the 1-D plug flow assumption to break down.

Combustion products, in particular soot precursors, collected from the tube reactor exit plane were analyzed using a gas chromatograph and mass spectrometer (GC/MS system). Extensive comparisons between the experimentally measured soot precursor data and computationally predicted results, using Sandia PREMIX reacting flow solver with a recently proposed detailed chemical kinetic model, showed reasonable agreement with the approach adopted here.

Contents

List of Figures

List of Tables

Nomenclature

Symbols

A - Cross sectional area of tube

$\overline{AF_a}$ - Actual air/fuel ratio

$\overline{AF_{st}}$ - Stoichiometric air/fuel ratio

c_p - Specific heat at constant pressure

D - Diameter of tube

h_c - Convective heat transfer coefficient

h_k - Specific enthalpy of kth species

k - Species index

M - Mach number

$\dot{m}$ - Mass flow rate

p - Pressure

p_0 - Stagnation pressure

$\dot{Q}_{adv}$ - Rate of advective heat transfer

$\dot{Q}_{cond}$ - Rate of heat conduction

r - Radius of tube

T - Temperature

T_0 - Stagnation temperature

U - Local fluid velocity

$\overline{v}$ - Cold average fluid velocity

$\dot{V}$ - Volumetric flow rate

$\dot{V}_{SLPM}$ - Volumetric flow rate in standard liters per minute

V_k - Diffusion velocity of kth species

W_k - Molecular weight of kth species

X_k - Mass fraction of kth species

Y_k - Mole fraction of kth species

Greek Symbols

ϵ - Emissivity

γ - Specific heat ratio

μ - Dynamic viscosity

$\dot{\omega}_k$ - Molar Production rate of kth species

ϕ - Equivalence ratio

ρ - Density

σ - Stefan Boltzmann constant

1 Introduction

1.1 Background

Soot emissions from gas turbine aircraft engines are known to have adverse effect on human health, especially near airports. Soot aerosols are also known to contribute to the nucleation of ice particles which form contrails. These contrails are the "vapor trails" that can be seen by an observer as planes fly overhead. Contrails can eventually grow into cirrus clouds, which have an uncertain and debatable effect on global surface temperatures [1, 2]. Because of these effects, it is important to understand the sooting regimes that lead to the formation of soot precursors in gas turbine exhaust. In the present study, two premixed reactors were used to better understand soot formation mechanisms and help in the mitigation of soot emission.

Soot forms in a combustor when excess amounts of fuel are unable to react with available oxygen to form CO_2 and H_2O. Pyrolysis occurs in the absence of oxygen and the fuel breaks down to smaller fragments such as C_2H_2 and C_3H_3. These species lead to the formation of polyaromatic hydrocarbons (PAH) [3]. C_2H_2, C_3H_3, and benzyl radicals are considered to be the key precursors to soot formation. The particles continue to grow through surface growth schemes presented by Mansurov [4]. Eventually the particles become so large ($\sim$ 30 nm) that their surface growth declines and they begin to coagulate with other large particles. In high pressure gas turbine engines, agglomerations of soot particles can reach sizes of $0.1 - 0.5$ μm [3].

1.2 Flow Reactors

One of the common ways to experimentally measure the evolution of premixed combustion products is through the use of a flow reactor. In a flow reactor, fuel, oxidizer, and diluents are continuously introduced into a heated cylindrical section with constant diameter and constant temperature. The flow rate can be varied to effectively

change the residence time. This ability to control temperature and residence time allows for the thorough investigation of conditions that contribute to the formation of soot precursors.

Ideally, flow reactors are considered to have plug flow conditions with negligible species and temperature gradients in the radial direction. Species are assumed to be perfectly mixed when they enter the reactor section and can therefore be modeled using a one-dimensional approximation.

Flow reactors come in many sizes and configurations, each with their own advantages and disadvantages. Due to more substantial mass flow rates, large diameter flow reactors require greater energy needs for heating and are thus more expensive to operate. One of the significant advantages of these larger reactors is the negligible wall collisions. Reactions caused by wall collisions are less understood than gas phase collisions and introduce uncertainty into the analysis. Another advantage of the large reactor is the greater accessibility of the flow for instrumentation and species probing. Small diameter flow reactors require limited flow and thus less energy to heat the mixture, making them inexpensive to operate. These reactors have the potential to run at high pressures more representative of conditions in gas turbine engines.

The configurations of flow reactors can vary in how they heat and mix the fuel and oxidizer. There is an inherent trade off in the ability to rapidly achieve target temperatures and to perfectly mix the fuel and oxidizer. If the fuel and oxidizer are mixed far upstream (Figure 1), achieving a target temperature takes time and portions of the residence will be at lower temperatures [5]. Alternatively, the diluent and oxidizer can be preheated to a target temperature and then introduce the (cold) fuel (Figure 2). The limited volume of fuel quickly reaches the desired temperature; however, a mixing length adds an awkward section where the residence time is difficult to quantify and spatial gradients exist. This mixing length can introduce offsets in experimental data when compared to computer models [6].
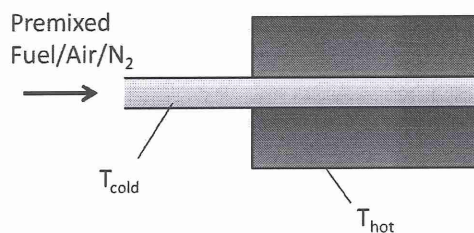
Figure 1: Non-preheated configuration
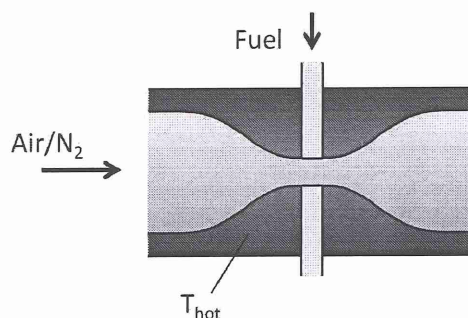
Figure 2: Preheated configuration

1.3 Outline

The purpose of this report is to analyze the first iteration of a new small diameter flow reactor configuration that attempts to correct the lag time to reach a target temperature through the use of a cartridge heated entry length. The ultimate objective of this reactor is to rapidly reach the target temperature profile. Also, it is desirable to run at a range of pressures, velocities (residence times), and temperatures. This range of conditions will allow for the exploration of sooting regimes.

A MATLAB program is written to model the heat transfer between the hot walls and the fluid passing through the reactor. The discussion of this code (see Section 3) examines the hardware requirements in order to achieve the desirable operating conditions and the limitations of the current iteration. Knowing the one dimensional temperature profile (modeled by the MATLAB program), Sandia's PREMIX com-

bustion code is used to predict species fractions at the tube exit [7].

The combustion products of the reactor are collected and analyzed with a gas chromatograph (GC) and gas chromatograph/mass spectrometer (GC/MS). Gas is sampled with a quartz probe at the exit of the reactor and transported to the system by a vacuum pump. The GC and GC/MS can both identify and quantify combustion products down to ppm levels. These results are compared with the PREMIX code results.

Finally, a flat flame burner similar to the "McKenna"[8] style is developed and sampled with the GC and GC/MS. This flat flame burner provides higher sooting conditions than the current iteration of the microflow reactor, thus it is useful to also compare its species profile with the PREMIX code results.

2 Experimental Setup

2.1 Overview

The experimental set up for the microflow reactor consists of a proportional-integral-derivative (PID) controlled fiber heater furnace with an inconel tube passing through it. Premixed fuel, air, and nitrogen are metered upstream and fed into the tube. As the mixture passes through the heated length of the tube, its temperature rapidly rises and the fuel begins to break down. Combustion products are probed at the exit of the tube and analyzed with a gas chromatograph (GC) and gas chromatograph/mass spectrometer combination (GC/MS). For further comparison with modeled data, samples are also collected and analyzed using a flat flame burner.

2.2 Mixture Control

Sierra Smart Trak 2 flow controllers and LabVIEW are utilized to administer the correct amount of fuel, oxidizer, and dilutant. Three flow controllers are used: 0.5 standard liters per minute (SLPM) for the fuel, 3 SLPM for air, and 5 SLPM for nitrogen. The fuel and nitrogen are supplied by large tanks from GTS Welco and Praxair. A compressor provides high pressure air which is dried and filtered en route to the flow controllers. The LabVIEW program originally written by Sarnacki [9] accepts inputs of cold velocity, fuel type, equivalence ratio, and nitrogen dilution percentage. It communicates the corresponding mass flows of fuel, air, and nitrogen to the flow controllers. The algorithm for calculating these flow rates with ethylene as the fuel is as follows:

The reaction of fuel and oxidizer (having unknown molar coefficients y and z which depend on nitrogen dilution and equivalence ratio) is given by,

$$C_2H_4 + y(O_2 + 3.76N_2) + zN_2 \rightarrow 2CO_2 + 2H_2O + (3.76y + z)N_2, \qquad (1)$$

where the equivalence ratio is defined as,

$$\phi = \frac{\overline{AF_{st}}}{\overline{AF_a}}, \tag{2}$$

which in terms of y is given by,

$$\phi = \frac{\overline{AF_{st}}}{4.76y}. \tag{3}$$

The desired mole fraction of nitrogen can be obtained from

$$X_{N_2} = \frac{3.76y + z}{1 + 4.76y + z}. \tag{4}$$

This results in two equations with two unkowns (y and z) that can be solved with knowledge of the fuel, equivalence ratio, and nitrogen mole fraction. The total volume flow rate is calculated from

$$\dot{V} = \pi \left(\frac{D}{2}\right)^2 \overline{v}. \tag{5}$$

The individual metered flow rates are then calculated by,

$$\dot{V}_{N_2} = \left(\frac{z}{1 + 4.76y + z}\right) \dot{V}, \tag{6}$$

$$\dot{V}_{air} = \left(\frac{4.76y}{1 + 4.76y + z}\right) \dot{V}, \tag{7}$$

$$\dot{V}_{fuel} = \left(\frac{1}{1 + 4.76y + z}\right) \dot{V}. \tag{8}$$

2.3   Tube Furnace

The goal of the tube furnace is to rapidly heat the fuel air mixture to a specified target temperature where it is held constant until probed at the exit. This is achieved through the use of PID controlled six heating zones (see Figure 3).

The first zone consists of a 1.25" long stainless steel block that is clamped to the

tube and heated by two Thermal Corp cartridge heaters. The cartridge heaters are 0.25" diameter, 3" long, rated for 200 W, and capable of temperatures up to 2000 F. A thermocouple is spot welded directly onto one of the cartridge heaters for PID control. Alumina insulation is placed over this "block heater" to mitigate energy lost to the atmosphere. The two cartridge heaters are wired in parallel and connected to a maximum 120 V power supply.

The next four zones are a multiple segment cylindrical fiber heater provided by Thermcraft. One 2-inch long segment is followed by three 4-inch long segments. Each segment consists of two half-cylindrical pieces of inner diameter 1.25" and outer diameter of 7.5". The 2-inch half-cylindrical pieces are rated at 100 W and 28.5 V while the 4-inch pieces are each rated at 200 W and 57.5 V. Each of the four segments is independently controllable via its own PID controller. The two halves of each 4-inch segment are wired in series and connected to a 120 V power supply. The two halves of the 2-inch segment are also wired in series; however, they are connected to a 60 V variac power supply (Superior Electric Co. Type 116B). The fiber heater is horizontally suspended by an aluminum trough. The temperatures of each segment are monitored by 6" long, 1/16" diameter unsheathed K type thermocouples from Omega Engineering Inc. The thermocouples are positioned between the halves of each segment such that the bead resides inside the cavity of the fiber heater.
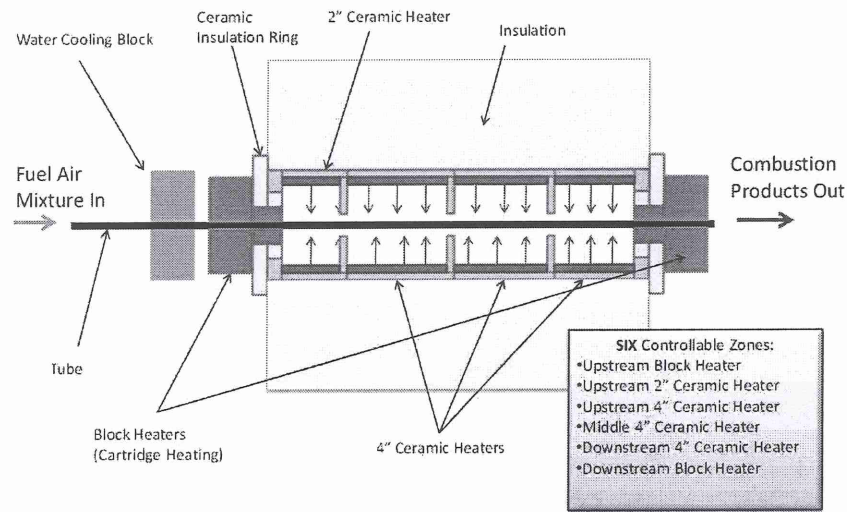
Figure 3: Six zone furnace

The final zone of the furnace is another block heater similar to that of the first zone. Again, two Thermal Corp cartridge heaters are used to heat a stainless steel block. A thermocouple is spot welded directly onto one of the cartridge heaters for temperature control purposes. Similarly, the cartridge heaters were wired in parallel with a 120 V power supply.

Before any of the heated zones, a copper water cooling block is clamped to the tube. This 2"x 2"x 2" cooling block serves to prevent heat from the furnace conducting upstream along the tube. Maintaining the steep temperature gradient at the entrance of the furnace is critical to achieving the stated goal of the system which is to have the fuel reside at a specified temperature for certain amount of time.

Six Omega CN77000 series PID controllers are used to control the six zones of the furnace. These PID controllers receive temperature signals from the six thermocouples and interact with six Omega SSR330DC25 solid state relays to power the block heaters and fiber heaters. The relays and PID controllers are mounted onto an aluminum panel for ease of viewing as well as cooling purposes (Figure 4).
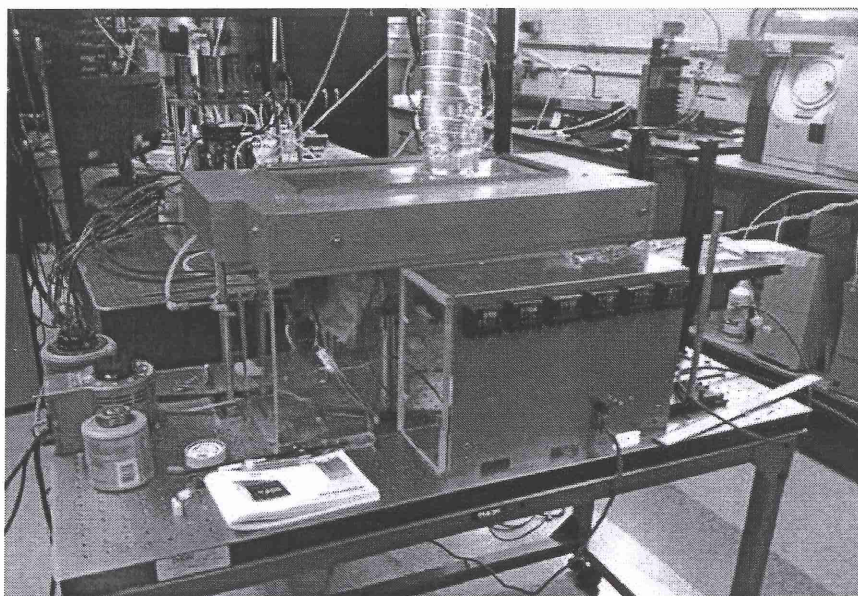
Figure 4: Photo of microflow tube reactor

2.4 Flat Flame Burner

The discrepancies in species concentrations between the tube reactor and the PRE-MIX model (see Section 5) motivated the use of an alternate set up for experimental measurements. This secondary experimental set up is a flat flame burner similar to the "McKenna" style burners. The flat flame burner (Figure 5) consists of two concentric copper cylinders. The inner cylinder contains the premixed fuel and air mixture while the outer cylinder provides a nitrogen shroud to ensure the flame is isolated from secondary reaction layers. The inner cylinder is water cooled with a copper coil. A 1/16" sintered porous disk is cemented at the outlet of the inner cylinder to provide a uniform and well-mixed flow while maintaining a low surface temperature. The burner is connected to a Newport Research Model 430 stage for accurate scanning of probed measurements. A similar probe mounting to that of the tube furnace is used for the flat flame burner. The probe is suspended and anchored above the burner while the height is changed by turning the dial on the burner's
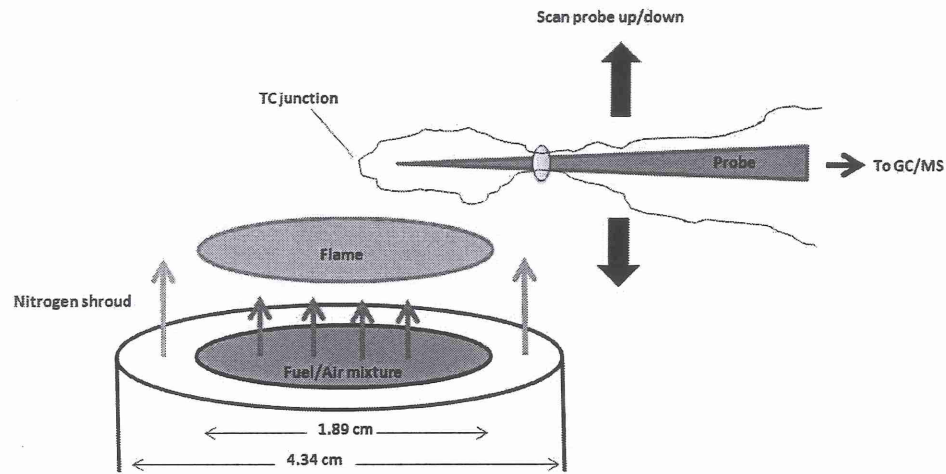
Figure 5: Flat flame burner set up

stage.

Temperatures are measured along with species by a thermocouple wire attached to the probe tip. An Omega 0.002" diameter bare wire type R (Pt-Pt13%Rh) thermocouple is cemented to the probe so the junction is suspended in front of the probe tip. This allows for simultaneous sampling and temperature measurements. Temperatures must be corrected for radiation losses as the wire is much hotter than its surroundings. The radiation correction performed is that discussed by Pitts, Braun, and Peacock [10]. It follows the equation:

$$T_g - T_j = \frac{\sigma \epsilon}{h_c}(T_j^4 - T_s^4),$$
(9)

where,

T_g = Gas temperature,

T_j = Thermocouple junction temperature,

σ = Stefan Boltzmann constant,

ϵ = Probe emissivity,

T_s = Temperature of surroundings.
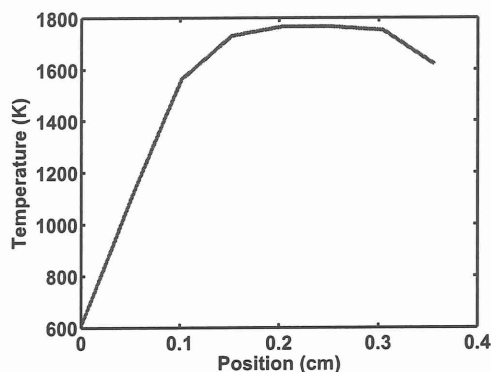
Figure 6: Corrected temperature profile for flat flame burner

The emissivity of the thermocouple wire is esitamted from Worthing [11]. The convection coefficient is calculated by the Nakai Okazaki equation for low Reynolds number flows [12]:

$$\overline{Nu}_D = \frac{1}{0.8237 - ln(Re_D Pr)^{0.5}} \tag{10}$$

where,

$$\overline{Nu}_D = \frac{\overline{h}_c D}{\lambda}. \tag{11}$$

This correction is necessary as the PREMIX code simulations are obtained with externally prescribed temperature profiles (Figure 6), i.e. TGIV mode (see Section 4).

2.5 Probe and Sampling

At the exit of the tube reactor and the flat flame burner, the exhaust gases are probed and analyzed using the GC and GC/MS. The design for sampling and transporting combustion gases from the exit of the reactor/burner to the GC inlet needs to address a few concerns. First of all, it needs to allow for the transport of potentially high molecular weight aromatic products without condensing. The most effective way to address this problem is by collecting the products at sub-atmospheric pressure. This system has been set up to sample at 0.5 atm. At 300 K and 0.5 atm, up to 28% Benzene or 263 ppm Napthalene can be collected without condensation.
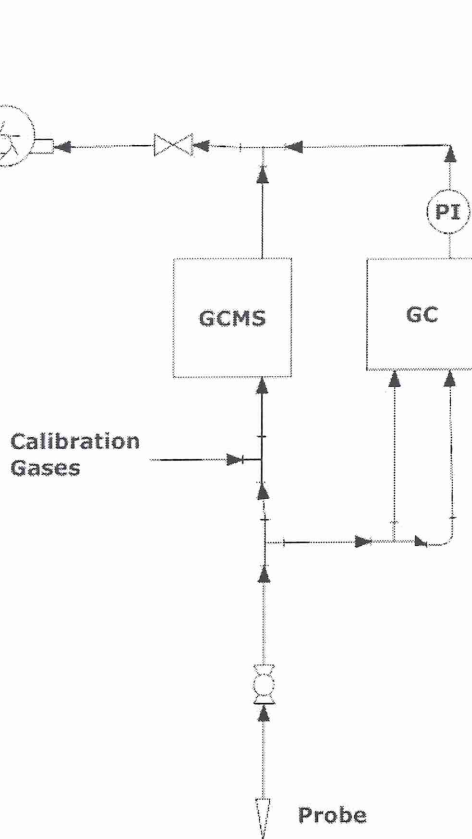
Figure 7: Downstream piping diagram

In order to achieve this low pressure, a pump is needed at the back end of the sampling system. The Welch Duo-Seal model 1397 vacuum pump is used for this experimental set up. Upstream of the pump, a needle valve is placed for controlling the pressure upstream. The pressure is measured and monitored just downstream of the GC sample loop so as not to potentially contaminate the entering sample. The needle valve is set so that the monitored pressure reads 7.35 psia when probe flow is closed off by a ball valve ("probe valve"). Figure 7 shows the plumbing set up.

The probe (Figure 8) should be of small enough diameter to be able to sample upstream of the incident flame at the end of the reactor tube. Due to its proximity to the downstream block heather, the probe needs to withstand very high temperatures.
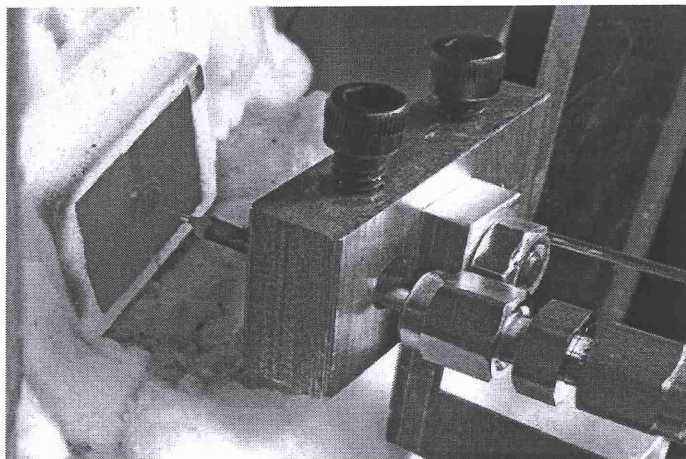
Figure 8: Photo of quartz probe

The probes used were made from a quartz tip attached to 1/8" stainless steel tube with Sauerizen #8. Sauerizen #8 is a high temperature cement that can withstand temperatures up to 2600 F. The quartz tips were made by a glass maker with slightly variable dimensions, but in general are conically shaped with a length of ∼20mm, inlet diameter of ∼200μm, and outlet diameter of ∼1.5mm.

2.6 Gas Chromatograph and Mass Spectrometer

Experimental data taken from the tube reactor and flat flame burner are analyzed with a gas chromatograph (GC) and gas chromatograph/mass spectrometer (GC/MS) system provided by Shimadzu Corp. This equipment allows for the identification and quantification of the species found in the combustion products of the reactor. The system must be calibrated with known standards of predetermined gas mole fractions to ensure the validity of collected data.

2.6.1 Gas Chromatography and Mass Spectrometry Overview

Gas chromatography is an analytical technique used to quantify species of gases. It can be used for a wide range of species, organic and inorganic, from the smallest and

most simple molecules such as hydrogen all the way to heavy polyaromatic hydrocarbons such as naphthalene and anthracene. GCs are commonly used in many industries including petrochemical, environmental, food and beverage, and automotive.

The initial goal of gas chromatography is to separate species as they travel through a column. This column is where the sample is introduced into the system. An inert, "mobile phase" carrier gas such as argon or helium is used to push the sample through the column. As the sample passes through the column, it interacts with a liquid "stationary phase" which coats column's inner walls. Depending on the solubility and adsorptive affinity of the sample with the stationary phase, species will partition themselves between the mobile and stationary phase. Lighter, small species often reside primarily within the mobile phase and thus travel through the column faster than large, heavy species which tend to cling to the stationary phase. The passage through a column with lengths of up to 100 m can create significant separation for even the most similar molecules. This process of compound extraction and separation from an analyte is termed elution [13].

Following elution, compounds are sent to a detector where they are quantified. Quantification takes the form of a chromatograph with peaks appearing at different times signifying when compounds have exited the column and been detected. Many types of detectors exist, but this paper will restrict its focus to the detectors found in the current system: the flame ionization detector (FID) and the thermal conductivity detector (TCD).

The FID (Figure 9) introduces the effluent to a hydrogen air flame where it is burned and produces ions. These ions are collected on an electrode where they produce a measurable current that forms the signal. Because the signal is dependent on this ion formation, inorganic compounds remain undetected by the FID as they are not burned in the presence of the flame. Another important characteristic of the FID is the destructive nature of its method of detection. Once the effluent is burned it
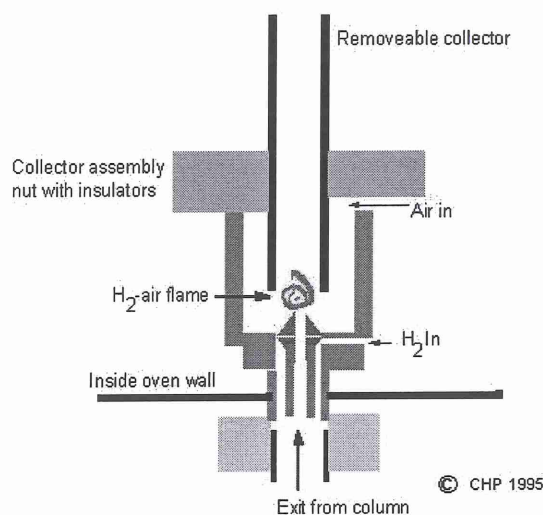
Figure 9: Schematic of flame ionization detector (Retrieved from http://www.chemistry.adelaide.edu.au/external/soc-rel/content/fid.htm)

can no longer be analyzed any further downstream [13].

The TCD (Figure 10) utilizes the difference in thermal conductivity between the pure carrier gas and eluate to create a signal quantifying the analyte. It consists of metal block with four cavities drilled into it. Filament wires are run through each of the cavities to form a wheatstone bridge. The column flow is sent through two of the cavities while pure carrier gas is sent through the other two. A current is then run through all of the filaments. The cavities with effluent have a lower thermal conductivity and thus their filaments experience a higher temperature as they struggle dumping heat to the block. The higher temperature increases the resistance of these filaments, causing an imbalance in the wheatstone bridge which is used as the signal. Because all compounds have a thermal conductivity regardless of flammability, the TCD is often used in quantifying inorganic species. Because of the TCD's nondestructive method of detection, the sample may be used downstream for further analysis.

Despite the TCD and FID's ability to quantify analytes, they fail to identify species with certainty. The use of a mass spectrometer compensates for this defi-
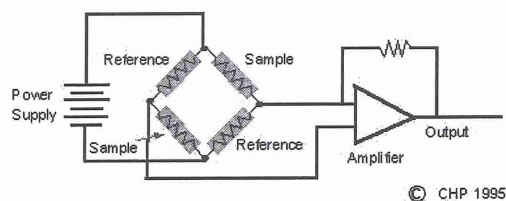
Figure 10: Schematic of thermal conductivity detector (Retrieved from http://www.chemistry.adelaide.edu.au/external/soc-rel/content/tcd.htm)
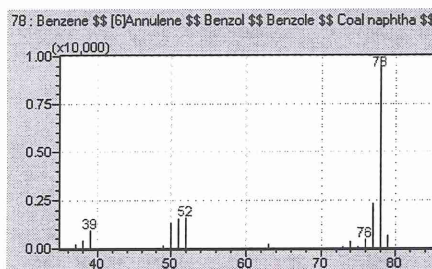
Figure 11: Sample mass spectrum for benzene

ciency. The MS accepts eluate from the GC column like the previously discussed detectors; however, this sample gas must first be vacuum pumped down to extremely low pressures ($10^{-5} - 10^{-6}$ torr). Once brought down to vacuum, the particles are ionized by a stream of electrons fired from a filament. This ionization occurs when fired electrons collide with the neutral analyte particles and eject an electron. These positively charged ions are then sorted by their mass to charge ratio (m/z) through the use of electromagnetic fields. Eventually ions reach a detector where they are quantified. The data is processed and output as a mass spectra (Figure 11). Peaks are created for each m/z read by the detector and scaled according to the mass ratio found in the largest quantity. The spectra are run through a database and compared to known spectra of chemical compounds. Matches confirm the identity of species [13].

This ability to sort analyte by mass ratio makes the combination of a GC and MS a very effective tool. The addition of an MS gives the user the power to further examine the makeup and identity of peaks that other detectors would see as a collective,
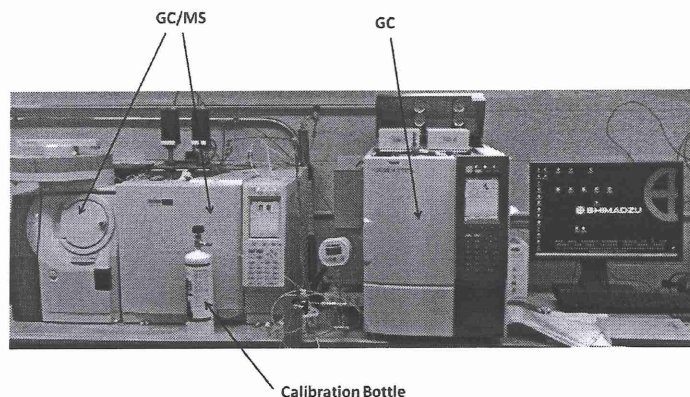
Figure 12: Photograph of GC and GC/MS system

anonymous signal. A single GC when coupled with a TCD or FID will never know with total certainty whether or not a seemingly independent peak caused by a single compound is actually two peaks merged together from two compounds that happen to coelute. The MS, on the other hand, has the ability to dig into this lone peak, examine the mass fragments formed within it, and identify and separate the contributions due to specific species. An alternative to using an MS for identifying species with certainty is the use of successive GCs where a second column is used to split up coeluting species.

2.6.2 GC and GC/MS System

The GC and GC/MS system used in the lab was purchased from Shimadzu Corp. It consists of a custom built model GC2014 and a model GCMS QP2010 Plus (Figure 12). The combination of these two pieces of equipment is intended to identify and quantify a wide range of species from combustion processes. It is desirable to measure simple hydrocarbons up to multi-ring PAH species as well as inorganic species such as hydrogen, nitrogen, oxygen, carbon dioxide, and carbon monoxide.

The custom GC 2014 contains two separate columns and three detectors. One

of the columns (Line 2) is connected to a TCD (TCD1) and is only used to measure molecular hydrogen. Because of hydrogen's low molecular weight, this column is specifically designed for slow elution and thus inappropriate for measuring larger species. The second column (Line 1) has two connected detectors, one FID (FID 1) and a second TCD (TCD2). This column and associated detectors are used for measuring nitrogen, oxygen, carbon dioxide, carbon monoxide, and small hydrocarbons (up to C_4). The temperatures in the columns can be programmed in the software's "method" file to tweak elution times if the need arises to try and separate two slightly overlapping peaks. In the event that two peaks significantly overlap and changes in column temperature fail at separation, the GC/MS may be used for analysis.

The GCMS QP2010 Plus is a combination gas chromatograph and mass spectrometer system. It contains only one column and uses the MS as its one and only detector. Because the eluate is analyzed in the MS at a pressure on the order of a billionth of an atmosphere, a strong pump is necessary. Shimadzu recommends and included an Edwards model RV3 two stage turbomolecular pump with this system. This GC/MS is designed to measure large hydrocarbons (C_4 and larger); however, it may also be used for smaller species that have peak overlaps in the GC. The more robust analytical abilities of the GC/MS inherently create more complexity for the user as more settings can be adjusted for fine tuned analysis. On top of being able to alter the column temperature program, the user can also modify how the MS detects mass fragments in the method file. The selected ion monitoring (SIM) capability may be imposed on top of the normal scan of total ion current (TIC). In utilizing the SIM, the MS is programmed to look for user-specified mass fragments over a desired temporal window. This focus on a select few fragments provides greater sensitivity in species measurements corresponding to those fragments. The scan over all mass fragments provides confirmation of species identity while the SIM provides a greater resolution for quantification. For this experiment, the MS was programmed to scan over entire

analysis as well as SIM for predominant mass fragments of larger hydrocarbons with available calibration standards (propane, propylene, butane, 1,3-butadiene, hexane, and benzene).

3   2–D Heat Transfer Model of Tube Reactor

3.1   Code Development

The small diameter of the reactor's tube makes experimentally measuring fluid temperatures along the heated length quite difficult. This inaccessability motivated the computational modeling of the heat transfer between the tube walls and the fluid. A two-dimensional heat transfer model was developed in MATLAB to predict fluid temperatures along the length of the reactor. The model accepts inputs of target temperature, upstream wall temperature profile, cold fluid velocity, and pressure and outputs a 2–D, radially symmetric temperature profile as well as a 1–D spatially averaged bulk temperature profile. The program makes the following assumptions:

1. Properties are calculated as if air were the fluid moving through the system (due to the extent of dilution).

2. Flow is laminar.

3. Flow is fully developed.

4. Fluid is an ideal gas.

5. Tube wall temperature is constant in radial direction.

The program in based on the analysis of the "thermal entry length problem" as discussed by Ribando [14]. The method involves applying an energy balance to annular control volumes. The domain is split into cells representing these control volumes with axial and radial coordinates of "i" and "j", respectively. For this 2-D model, the domain is divided into a 568x26 cell matrix which corresponds to a cell size of 0.00085 m by 0.0001 m. The energy equation is applied between the cells as follows:

$$\dot{Q}_{cond,in} - \dot{Q}_{cond,out} + \dot{Q}_{adv,in} - \dot{Q}_{adv,out} = 0, \tag{12}$$

where,

- $\dot{Q}_{cond,in}$ = Rate of heat conduction in,

- $\dot{Q}_{cond,out}$ = Rate of heat conduction out,

- $\dot{Q}_{adv,in}$ = Rate of advective heat transfer in,

- $\dot{Q}_{adv,out}$ = Rate of advective heat transfer out.

Note that it is assumed that axial conduction terms are small and negligible compared to the others.

Using first order finite differencing, the energy equation,

$$\rho c_p U \frac{\partial T}{\partial x} = \frac{k}{r} \frac{\partial}{\partial r} \left(r \frac{\partial T}{\partial r} \right), \tag{13}$$

can be written as:

$$-2\pi \lambda r_{j-1} \frac{T_{i,j} - T_{i,j-1}}{dr_{j-1}} dx + 2\pi \lambda r_j \frac{T_{i,j+1} - T_{i,j}}{dr_j} dx +$$
$$\rho c_p U_j \pi (r_j^2 - r_{j-1}^2) T_{i-1,j} - \rho c_p U_j \pi (r_j^2 - r_{j-1}^2) T_{i,j} = 0. \tag{14}$$

In order to solve this equation for the temperature at each location, the energy equation must be in the form:

$$DU(j)T_{i,j+1} + D(j)T_{i,j} + DL(j-1)T_{i,j-1} = B(J). \tag{15}$$

After rearrangement:

$$(2\lambda r_j \frac{dx}{dr})(T_{i,j+1}) + (-2\lambda r_{j-1}\frac{dx}{dr} - 2\lambda r_j \frac{dx}{dr} - \rho c_p U_j(r_j^2 - r_{j-1}^2))(T_{i,j})+$$

$$(2\lambda r_{j-1}\frac{dx}{dr})(T_{i,j-1}) = (-\rho c_p U_j(r_j^2 - r_{j-1}^2))(T_{i-1,j}), \quad (16)$$

where,

$$DU(j) = 2\lambda r_j \frac{dx}{dr}, \tag{17}$$

$$D(j) = -2\lambda r_{j-1}\frac{dx}{dr} - 2\lambda r_j \frac{dx}{dr} - \rho c_p U_j(r_j^2 - r_{j-1}^2), \tag{18}$$

$$DL(j-1) = 2\lambda r_{j-1}\frac{dx}{dr}, \tag{19}$$

$$B(j) = (-\rho c_p U_j(r_j^2 - r_{j-1}^2))(T_{i-1,j}). \tag{20}$$

These coefficients form a tridiagonal system of equations that can be written as the matrix equation:

$$
\begin{bmatrix}
D(1) & DU(1) & 0 & \cdots & & \cdots & 0 \\
DL(1) & D(2) & DU(2) & 0 & & \cdots & \vdots \\
0 & DL(2) & D(3) & \ddots & & \cdots & \vdots \\
\vdots & 0 & \ddots & \ddots & & \ddots & \vdots \\
\vdots & \vdots & \vdots & \ddots & & \ddots & DU(j_{max-1}) \\
0 & \cdots & \cdots & & \cdots & DL(j_{max-1}) & D(j_{max})
\end{bmatrix}
\begin{bmatrix}
T(1) \\
T(2) \\
\vdots \\
\vdots \\
T(j_{max-1}) \\
T(j_{max})
\end{bmatrix}
=
\begin{bmatrix}
B(1) \\
B(2) \\
\vdots \\
\vdots \\
B(j_{max-1}) \\
B(j_{max})
\end{bmatrix}
$$

This equation can be solved by Gaussian elimination with partial pivoting through the use of the SGTSV routine from LAPACK: Linear Algebra PACKage [15]. Every time this function is called, it solves for the radial temperature array at a given axial location. Every time the program iterates through a new step (axial location), SGTSV is called again to calculate the next temperature array.

In the more basic model described by Ribando [14], all of the fluid properties are assumed to be constant. This code for the microflow reactor has been adapted to account for variable properties such as thermal conductivity, viscosity, density, and specific heat. All four of these properties are given dependencies based on temperature and pressure. Properties such as thermal conductivity and viscosity are calculated using relations by Bahadori [16]. For each property, Bahadori gives a (different) four by four matrix of coefficients,

$$
\begin{bmatrix}
A_{11} & \cdots & A_{14} \\
\vdots & \ddots & \vdots \\
A_{41} & \cdots & A_{44}
\end{bmatrix},
$$

that are first condensed into a vector by the following pressure equations:

$$
a_1 = A_{11} + A_{12}p + A_{13}p^2 + A_{14}p^3, \tag{21}
$$

$$
a_2 = A_{21} + A_{22}p + A_{23}p^2 + A_{24}p^3, \tag{22}
$$

$$
a_3 = A_{31} + A_{32}p + A_{33}p^2 + A_{34}p^3, \tag{23}
$$

$$
a_4 = A_{41} + A_{42}p + A_{43}p^2 + A_{44}p^3. \tag{24}
$$

The final relations are given by:

$$
ln(\lambda) = a_1 + \frac{a_2}{T} + \frac{a_3}{T^2} + \frac{a_4}{T^3}, \tag{25}
$$

$$
ln(\mu) = a_1 + \frac{a_2}{T} + \frac{a_3}{T^2} + \frac{a_4}{T^3}. \tag{26}
$$

The density is calculated from the ideal gas law:

$$p = \rho RT. \tag{27}$$

The specific heats are calculated using a sixth order curve fit of tabulated specific heats for air at various temperatures from Mills [17].

Because these properties are a function of temperature and the code is simultaneously solving for temperature, iteration is introduced into the code. For each new axial location, a temperature is guessed based on the previous step. Properties are calculated based on this guessed temperature and the code proceeds in calculating the temperature array for the current axial location. New guesses are created if the difference between the calculated temperature at any radial location and the guessed temperature is greater than 0.1 K.

All of the aforementioned analysis requires the knowledge of the surface temperature of the tube. Since the fiber heater is PID controlled and can maintain a specified temperature (target temperature), the more interesting area to examine surface temperature is at the upstream end of the tube where the block heater causes steep temperature gradients. A wall temperature profile is created by probing seven wall temperatures that traverse through the block heater along the tube. These points are linearly connected and the remainder of the wall profile is assumed to be the target temperature.

3.2   Model Analysis

With the MATLAB code described above, the effect of changing the pressure and velocity of the fluid can be examined for various temperatures. This section will examine these effects for a target temperature of 950 K with cold average velocities ($\overline{v}$) of 0.5 m/s, 2 m/s and pressures of 1 atm and 10 atm. A baseline case is given with a cold average velocity of 0.5 m/s and a pressure of 1 atm can be seen in Figure 13.
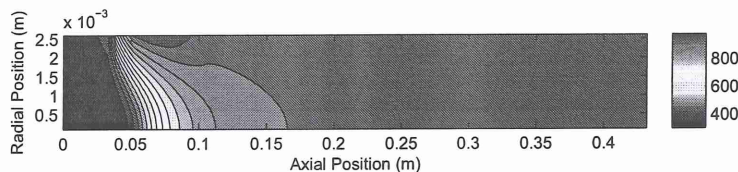
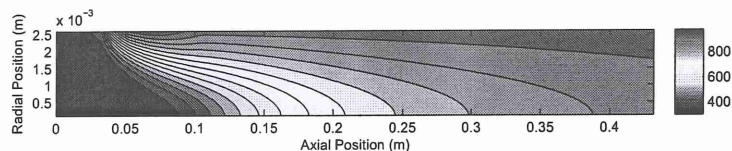Figure 13: Target 950 K profile with $\overline{v} = 0.5$ m/s, p = 1 atm

Figure 14: Target 950 K profile with $\overline{v} = 2$ m/s, p = 1 atm

The model is first run at target temperatures of 950 K while keeping the pressure constant (1 atm) and varying the cold average velocity. As can be seen in the Figure 14, when the velocity is increased, the cold core of the fluid extends further into the tube causing large radial temperature gradients. The reason for this extension of the cold core when increasing the velocity can be understood when examining the energy equation used in the model. When the cold average velocity is increased, the subsequent increase in local velocity U_j causes the two advection terms begin to dominate the conduction terms. Because the energy is being preferentially transferred from the upstream cell, rather than the radially adjacent cell, it takes longer for the core to see an increase in temperature. Since the fluid is being heated from the walls and not an upstream source, it is necessary that the conduction terms play a more dominant role in this energy equation.

The model was then run at target temperatures of 950 K while keeping the average velocity constant (0.5 m/s) and varying the pressure. As can be seen in the Figure 16, increasing the pressure (with constant velocity) in the model has a very similar effect to that of raising the velocity and keeping the pressure constant. Again, this can be traced back to the energy equation. As with velocity, the advection terms in the energy equation contain a density term. Increasing the pressure of the fluid
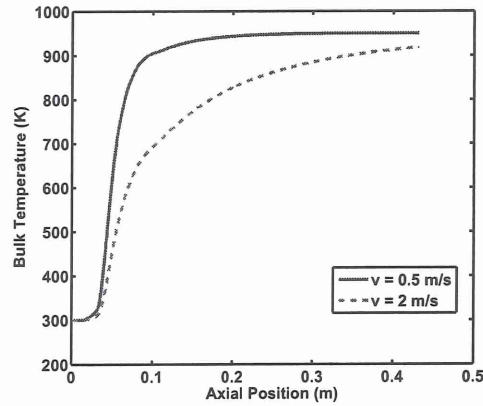
Figure 15: Target 950 K bulk temperature profile with $\bar{v} = 2$ m/s, p $= 1$ atm
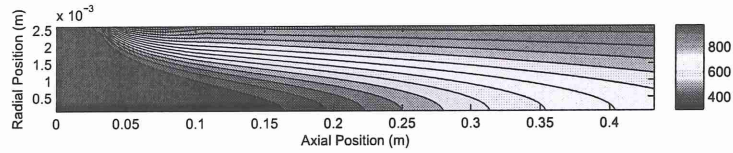

Figure 16: Target 950 K profile with $\bar{v} = 0.5$ m/s, p $= 10$ atm

will increase its density according to the ideal gas law. Every time the pressure is increased, the subsequent increase in density will again cause the advection terms to take precedent over the conduction terms. As discussed above, this will exacerbate the issue of having a cold core penetrate far downstream and the creation of significant radial temperature gradients.

Now that the effects of changing the pressure and velocity of the flow are well understood, it is important to examine what hypothetical wall profiles would be necessary to achieve a "top-hat" temperature profile for the desired range of conditions. A "top-hat" profile is defined as a bulk temperature reaching 95% of the target temperature within 0.1 m of entering the reactor. These extreme profiles are created for a target temperature of 1150 K as it is the highest desired temperature for this experimental set up. The wall profiles are then compared to the attainable profiles using the current hardware.

The first wall profile is created under the most extreme conditions which are
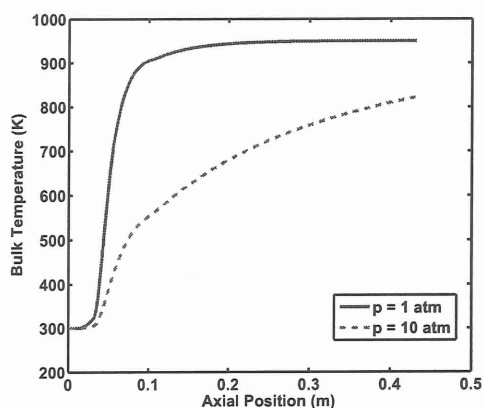
Figure 17: Target 950 K bulk temperature profile with $\bar{v} = 0.5$ m/s, p = 10 atm

a velocity of 2 m/s and a pressure of 10 atm. The needed wall profile, resulting bulk temperature profile, and 2-D temperature plot are visible in Figure 18. The wall profiles needed for other velocities and pressures are shown in Figure 19 and Figure 20, respectively.

The hottest wall profile available can be seen in Figure 21. Clearly, with the current hardware, it is impossible to achieve a "top-hat" profile for high temperatures, velocities, and pressures.

It is also important to note that even if these extreme wall temperatures were available, the two dimensional profile exposes a major flaw in the temperature profiles. Despite the fact that the bulk temperature profile may reach a desired value, severe temperature gradients exist in the radial direction. Ideally, there should be no radial dependence on temperature, resulting in minimal species gradients in the radial direction. These "hot spots" close to the wall will locally accelerate reactions and shatter any hopes of having radially independent species concentrations. These deficiencies in the current experimental setup need to be addressed if a wide range of temperatures, residence times, and pressures are to be explored.

Figure 18: Required wall temperature to achieve 1150 K bulk temperature at $\overline{v} = 2$ m/s, p = 10 atm

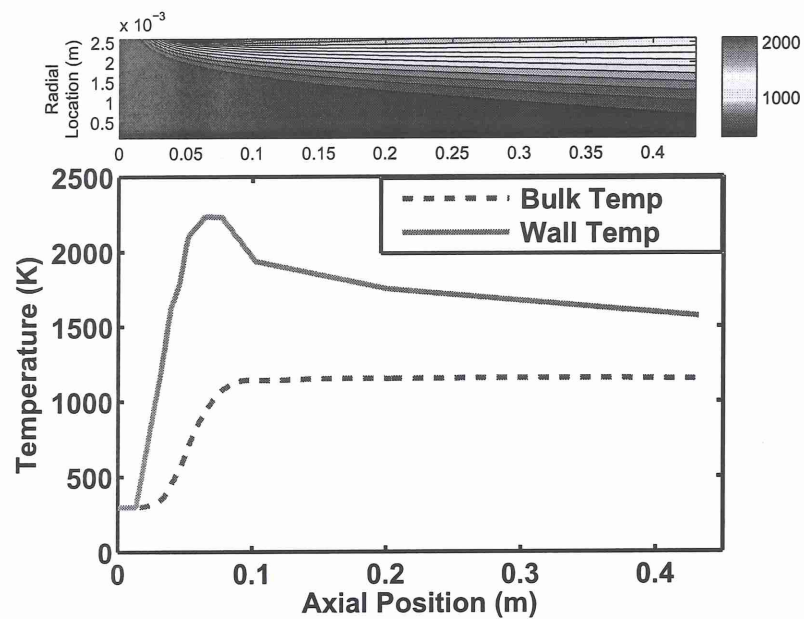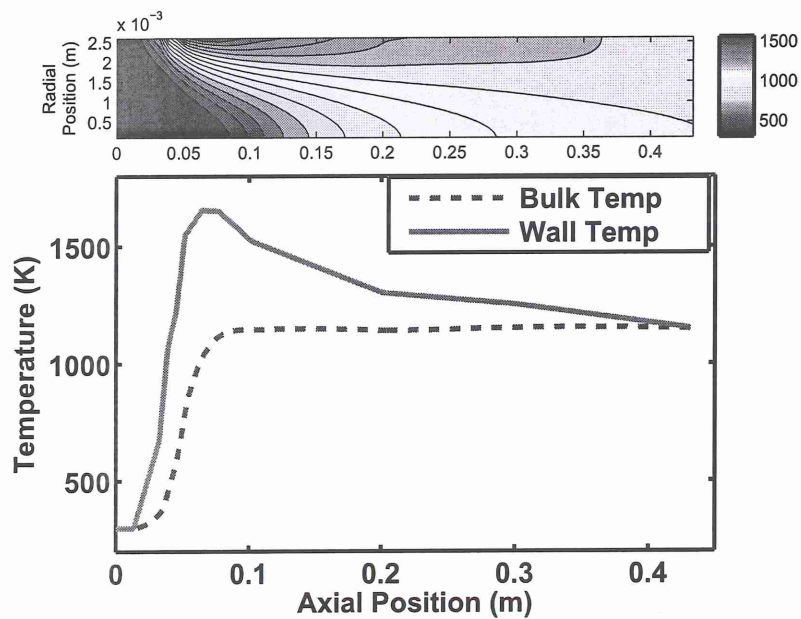Figure 19: Required wall temperature to achieve 1150 K bulk temperature at $\overline{v} = 2$ m/s, p = 1 atm
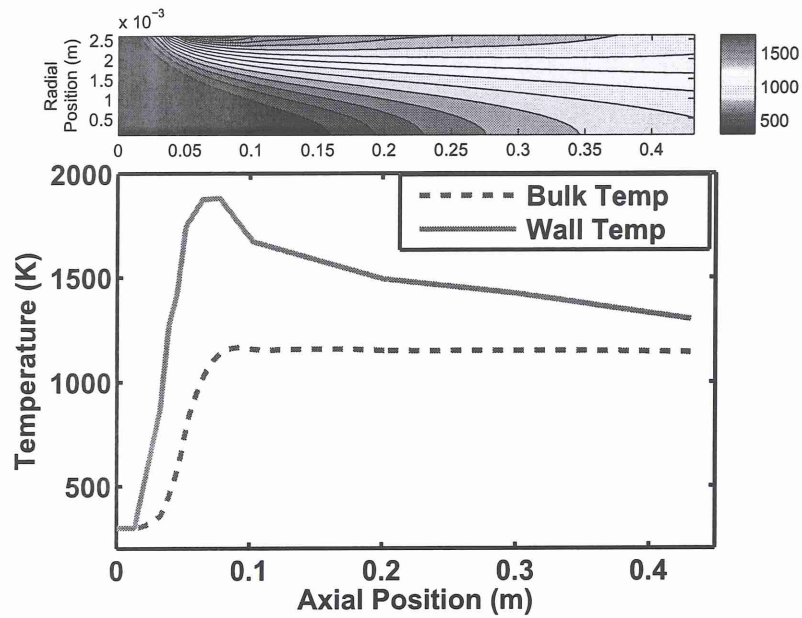
Figure 20: Required wall temperature to achieve 1150 K bulk temperature at $\overline{v} = 0.5$ m/s, p = 10 atm
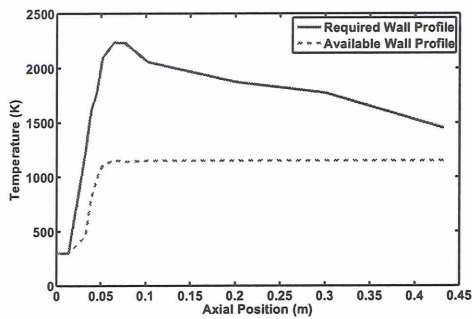

Figure 21: Comparison of available wall temperature profile with required wall temperature profile needed to attain "top-hat" profile over desired conditions $\overline{v} = 2$ m/s, p = 10 atm

4   1-D PREMIX Reacting Flow Simulation

The one-dimensional reacting flow solution algorithm developed by Sandia National Laboratories, which includes complex interaction of flow residence time (convective and diffusive) and finite rate chemistry, is extensively used in the literature [7]. Specifically, numerically predicted species concentrations are used to optimize and validate chemical kinetic models.

Here, experimentally measured species concentrations or mole fractions are compared to the Sandia PREMIX chemical kinetic model. The PREMIX code calculates species and temperature profiles for one-dimensional, isobaric, laminar, steady premixed flames. The program has the capability to solve for burner-stabilized or freely propagating flames with either a fixed, user-defined temperature profile or a calculated profile from solving the energy conservation equation. The equations governing the 1-D premixed reacting flow are as follows:

Continuity:

$$\dot{m} = \rho \bar{v} A, \tag{28}$$

Energy:

$$\dot{m}\frac{dT}{dx} - \frac{1}{c_p}\frac{d}{dx}\left(\lambda A\frac{dT}{dx}\right) + \frac{A}{c_p}\sum_{k=1}^{K}\rho Y_k V_k c_{pk}\frac{dT}{dx} + \frac{A}{c_p}\sum_{k=1}^{K}\dot{\omega}_k h_k W_k = 0, \tag{29}$$

Species:

$$\dot{m}\frac{dY_k}{dx} + \frac{d}{dx}\left(\rho A Y_k V_k\right) - A\dot{\omega}_k W_k = 0 \quad (k = 1, ..., K). \tag{30}$$

Chemical reaction rate source terms ($\dot{\omega}_k$) and transport properties (λ, c_p, V_k, etc.) are calculated from the Sandia CHEMKIN[18] and TRANSPORT[19] packages, respectively. The PREMIX code is run through a UNIX operating system where results can be exported to MATLAB for analysis. The tube reactor is best modeled as a burner-stabilized flame with a given temperature profile. This type of problem is

specified in the code through the keywords "BURN" and "TGIV". "BURN" informs the code to solve a burner stabilized flame while "TGIV" means the user must supply a temperature profile. The necessary inputs for the program include the pressure (atm), mass flowrate ($\frac{g}{cm^2 \cdot s}$), input species mole fractions, and the temperature profile as a matrix of locations (cm) and temperatures (K).

Since the code only solves for one-dimensional species profiles, it is expected that the input temperature profile is required to be one-dimensional. The one-dimensional temperature profile entered into the PREMIX code is the bulk temperature profile output by the heat transfer MATLAB model. This one-dimensional approximation is only valid for minimal radial temperature gradients as large radial temperature gradients introduce a second dimension to the analysis. This two-dimensional nature makes the comparison with a one-dimensional species solver inappropriate. For this reason, the validity of the one-dimensional bulk temperature needs to be weighed against its corresponding two-dimensional temperature profile.

As discussed in the previous section, the current experimental set up has difficulty attaining a "top-hat" profile; however, since the PREMIX code receives any user-defined profile, it can still be used for model comparison. As long as the MATLAB heat transfer code adequately produces a one-dimensional profile that correctly describes the system, this profile can be input into PREMIX for species analysis. Experimental data was collected for the following inflow conditions:

- Mole fraction nitrogen $X_{N_2} = 0.9$,

- Equivalence ratio $\phi = 2$,

- Target temperature $T_{target} = 1050K$,

- Cold velocity $\bar{v} = 2m/s$.

The target temperature of 1050 K corresponds to the PID controllers set to the following temperatures (K):
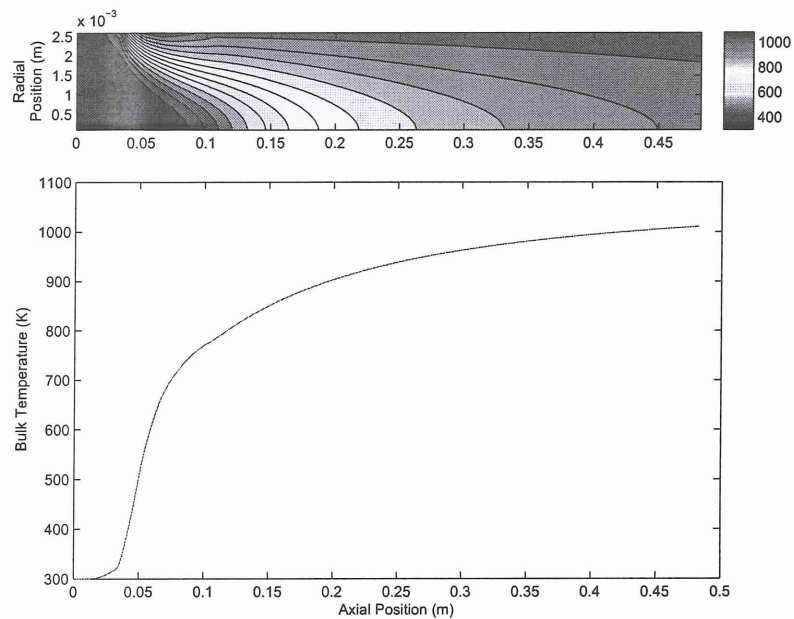
Figure 22: 1-D bulk temperature profile for PREMIX input and corresponding 2-D contour

- Upstream block heater: 1220,

- Fiber Heaters (4): 1050,

- Downstream block heater: 1148[1].

Running the MATLAB heat transfer code with these inputs creates a one-dimensional bulk temperature profile as seen in Figure 22. This bulk temperature profile is then entered into PREMIX along with the pressure, mass flow rate, and initial mole fractions. The output species profiles are summarized in Figures 23 - 25.

It is readily apparent from the figures that the breakdown of the fuel and subsequent chemical reactions were only beginning to occur at about three quarters of the tube's length. This is due to the inability of the upstream block heater to adequately heat the fluid to high enough temperatures where reactions begin to take place. A

---

[1]Downstream block heater temperature chosen so average fluid temperature along its length is equal to the target temperature

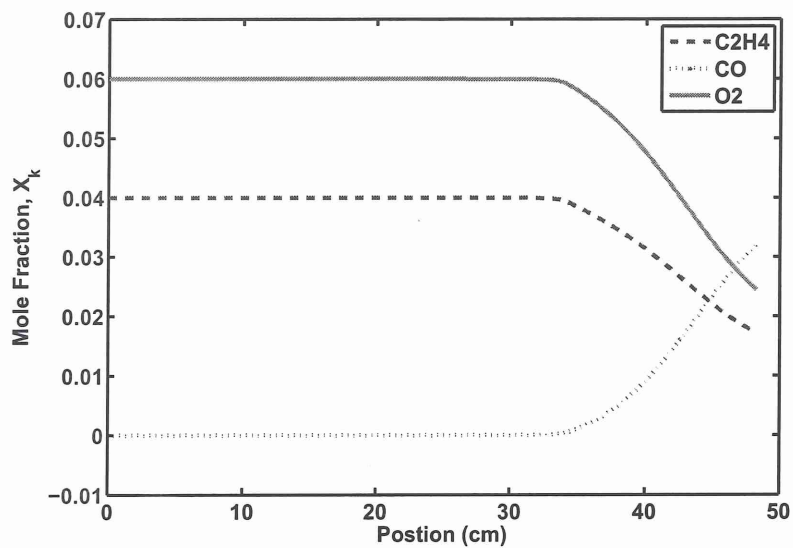Figure 23: Major species mole fractions vs. distance for $\phi = 2$, $(X_{N_2})_{in} = 0.9$, p = 1 atm, $T_{target} = 1050K$
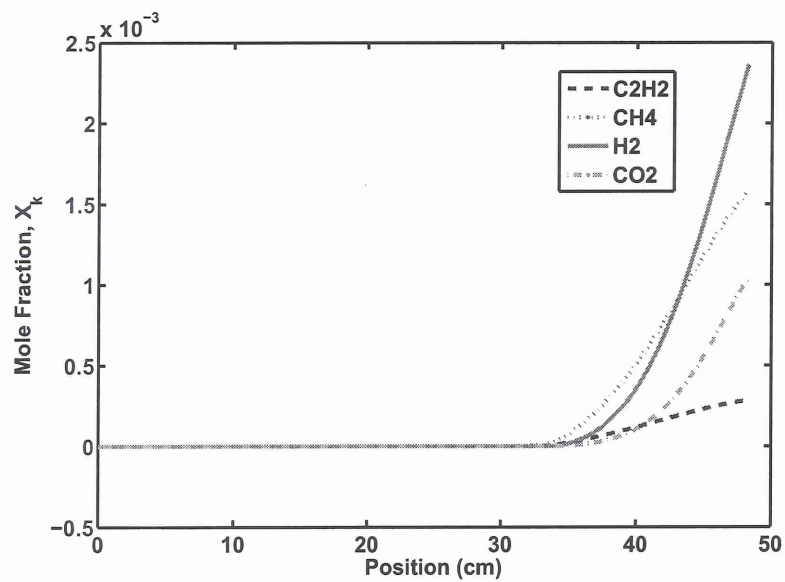

Figure 24: Minor species mole fractions vs. distance for $\phi = 2$, $(X_{N_2})_{in} = 0.9$, p = 1 atm, $T_{target} = 1050K$
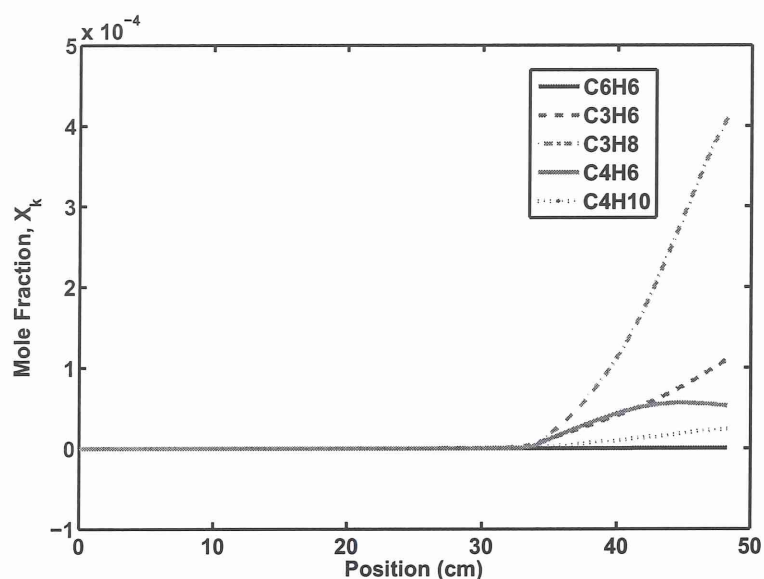
Figure 25: Trace species mole fractions vs. distance for $\phi = 2$, $(X_{N_2})_{in} = 0.9$, p = 1 atm, $T_{target} = 1050K$

cold, inert core of fluid penetrates deep into the reactor. As the bulk temperature eventually reached above about 950 K, intermediate species and products began to form.

The figures clearly show that the current experimental set up is unable to heat the fluid to temperatures where soot precursors such as acetylene and benzene form in appreciable amounts. By the exit of the tube, only 280 ppm of acetylene and 250 parts per billion (ppb) of benzene are formed. The purpose of the microflow tube reactor is to explore sooting regimes with tight control of temperatures and residence times. New iterations to the experimental set up will be necessary to meet these goals.

Because the probe is set up to collect only combustion products from the exit of the tube, only the last species mole fractions values from the PREMIX simulation are of concern with regards to experimental validation. The final values of these species profiles will be compared to experimental GC measurements in the subsequent section.

The 1-D Sandia PREMIX code is also run for the flat flame burner using the radiation corrected temperature profile from Figure 6. Results and discussion of the PREMIX code for the flat flame burner will also be presented in the following section alongside the GC and GC/MS experimental data.

5 GC/MS Calibration and Experimental Results

As discussed in Section 2.6, before any experimental data is collected, the GC and GC/MS must be calibrated. Without correct calibration, analyzed data is quantitatively meaningless. This system is primarily calibrated using Air Liquide SCOTTY™ Specialty Calibration Gases. The following table summarizes calibration gases used, their standard (molar) fraction, as well as their uncertainty:

Table 1: Calibration Levels (SCOTTY™ tanks)

Species	Level#1	Level#2
C_2H_4	1000 ppm $\pm$ 2%	10 ppm $\pm$ 5%
C_2H_2	1000 ppm $\pm$ 2%	
CH_4	1000 ppm $\pm$ 2%	10 ppm $\pm$ 5%
CO	1010 ppm $\pm$ 2%	10.1 ppm $\pm$ 5%
CO_2	1000 ppm $\pm$ 2%	10 ppm $\pm$ 5%
O_2	1000 ppm $\pm$ 2%	
C_6H_6	1000 ppm $\pm$ 2%	20.5 ppm $\pm$ 10%
C_2H_6	101 ppm $\pm$ 10%	
C_3H_6	1000 ppm $\pm$ 2%	
C_3H_8	101 ppm $\pm$ 10%	
C_4H_6	101 ppm $\pm$ 5%	
C_4H_10	101 ppm $\pm$ 10%	
C_6H_{14}	102 ppm $\pm$ 10%	

These calibration gases are introduced into the system via a "T" joint in Figure 7 labeled "Calibration Gases". While gases are being introduced, the valve nearest the probe is shut to ensure no gas escapes from the tip. The Welch vacuum pump is turned on and the pressure is adjusted via the inline needle valve to a value of 7.35 psia. The calibration gas is then cracked open two or three times to flood the system with the standard gas selected. The pressure will initially spike due to this sudden introduction of gas but will eventually settle back to 7.35 psia. Once the desired pressure is reached, analysis is begun in the GC or GC/MS (depending on which is used to measure the species being calibrated). This procedure is done for all calibration bottles.

Calibration curves are linearly extrapolated indefinitely to very high concentrations regardless of how low the concentration is of their calibration levels from the SCOTTY™ tanks. This extrapolation can lead to errors for species measured in high concentrations. These species, which include oxygen, nitrogen, and ethylene, are further calibrated using specified flow-controlled concentrations and atmospheric air. The first of these calibrations is a mixture of $90\%(molar)N_2$, $6\%O_2$, and $4\%C_2H_4$. The second calibration is simply dry air ($79\%N_2$, $21\%O_2$) run through the system. The addition of these two mixtures adds a third level of calibration to C_2H_4, a second and third level to O_2, and a first and second level to N_2. Both of these mixtures are introduced to the system via the sampling probe and not the calibration port. The probe valve is left open while sample is pumped into the system. After a couple minutes[1], the probe valve is shut. Once the probe valve is shut, the pressure will again decrease back to 7.35 psia at which point the desired calibration is performed.

Once all calibration runs are completed in the GC and GC/MS, calibration curves are created in the software for the corresponding species. Calibration curves are chosen to be lines connecting each point (level) of calibration. The mole fraction of analyte species is taken to be the linear interpolation of the experimental chromatograph peak area with the peak areas of the closest calibration standards.

5.1 Tube Reactor Results

As discussed in the previous section, the GC and GC/MS data collection took place for the following conditions:

- Mole fraction nitrogen $X_{N_2} = 0.9$,

- Equivalence ratio $\phi = 2$,

- Target temperature $T_{target} = 1050K$,

---

[1]See Appendix A for analysis of probe flow.

- Cold velocity $\overline{v} = 2m/s$,

with the PID controllers at the following settings (temperature in K):

- Upstream block heater: 1220,

- Four Fiber Heaters: 1050,

- Downstream block heater: 1148.

Once the furnace temperature reaches equilibrium, the probe is placed at the exit of the tube as seen in Figure 8. With the probe valve and calibration inlet closed, the Welch vacuum pump is turned on and the needle valve adjusted until a pressure of 7.35 psia is reached. At this point, the probe valve is opened and sample will begin to fill the lines to GC and GC/MS. After a couple minutes, the lines will be completely flooded and the probe valve is closed. Once the pressure gauge falls back down to 7.35 psia, sample collection is begun in the GC and/or GC/MS software.

Figure 26(a) - Figure 26(g) shows data from sixteen experimental runs with only the most prominant and calibrated species shown. For each experimental run, the experimental data is represented by the individual bar graphs, while the solid line represents the predicted value from PREMIX code. The dashed lines bound the experimental data to plus/minus one standard deviation. Of the eight measured species, four of the species' modeled PREMIX mole fractions fell within one standard deviation of the mean experimental values. These species were ethylene, methane, nitrogen, and oxygen. Of the four remaining species, acetylene narrowly missed the standard deviation window with a 19.24% error. The mean carbon monoxide mole fraction deviated from the PREMIX result by less than 25%. The last two species, carbon dioxide and hydrogen, had extremely large errors of 1055% and 217% respectively. One source of error, especially for that of CO, is the fact that the highest calibration level was much smaller than the experimental measurement. The calibration curve

is linearly extrapolated to higher concentrations; however, the true calibration curve may not be perfectly linear. The largest fraction of CO for calibration was 1010 ppm (for safety reasons) and the experimentally extrapolated mean fraction was over 24,000 ppm. This linear extrapolation may not be valid for concentrations 24 times higher than the standard. A further source of error may be caused wall collisions and/or a catalytic effect of having an inconel tube of small diameter. Trace species mole fractions may be altered significantly by wall collisions, especially if they are catalytic. Further work will explore and hopefully account for these effects.
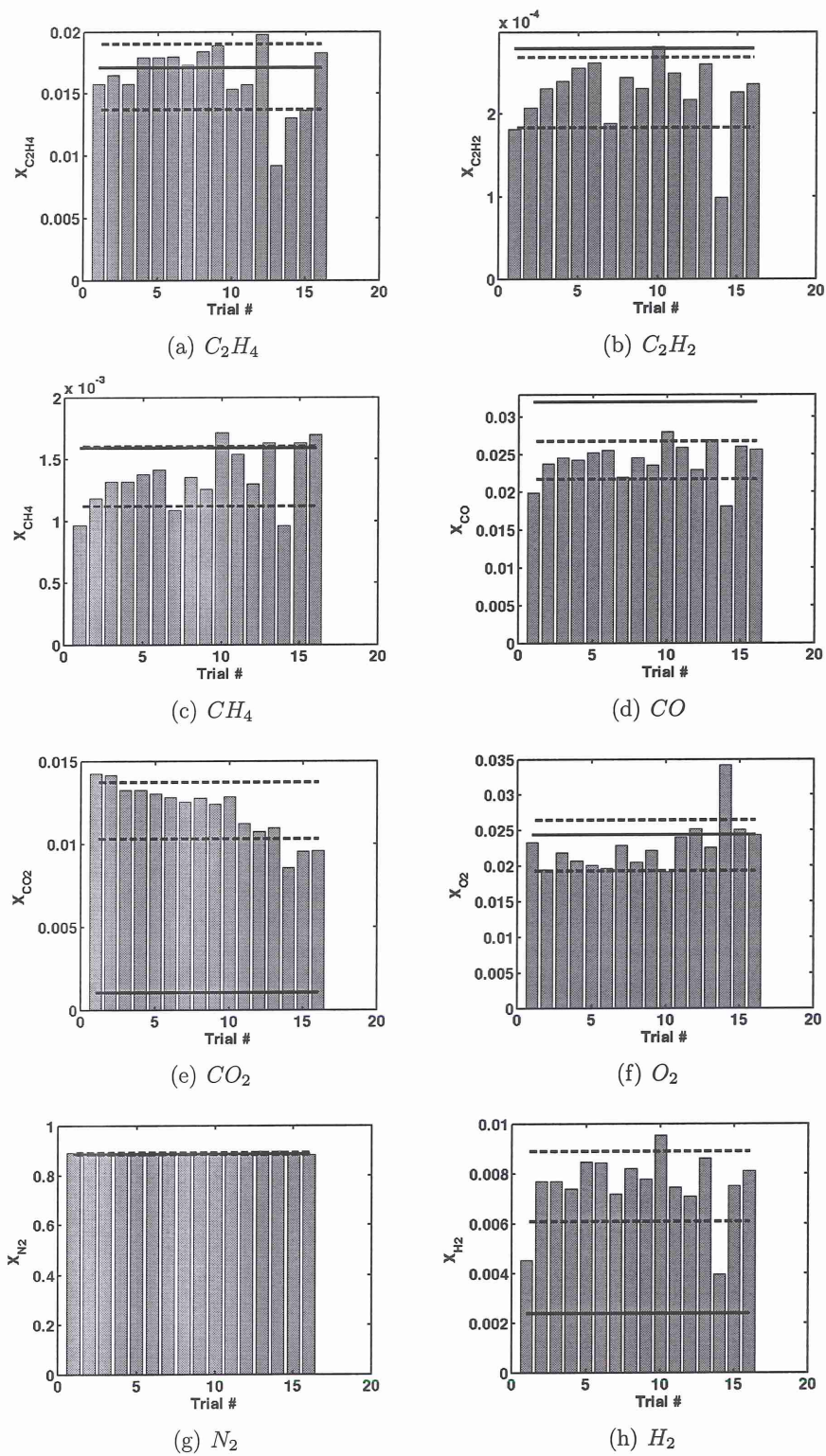
Figure 26: Experimentally measured species mole fractions and their uncertainty bounds over 16 runs at $\phi = 2$, $X_{N_2} = 0.9$, $T_{target} = 1050K$, p = 1 atm, $\overline{v} = 2m/s$. Also shown are predicted values from the PREMIX code.

5.2   Flat Flame Burner Results

Because of the uncertainties associated with wall effects in the tube reactor, an alternative and somewhat simple flat flame burner was considered to assess the GC and GC/MS system. Previously, such burners have been used extensively to analyze flame structures. The data for the flat flame burner was collected under the following conditions:

- $\phi = 2$,

- Cold velocity = 18 cm/s,

- Shroud velocity = 16 cm/s.

Species and temperatures are measured at eight locations starting from the surface of the burner and increasing in 0.02" increments. GC and GC/MS samples are collected using similar methodology to that of the tube furnace; however, now it is taken at eight different spatial locations as opposed to just one. The corrected temperature profile (Figure 6) is given as input to the PREMIX code for predicting species mole fractions and comparison with those experimentally measured by GC and GC/MS. The experimental and modeled species data are summarized in Figure 27(a) - Figure 27(n).

The first and most readily apparent difference between the experimental and modeled data is the fact that the experimental data failed to match the model at the surface of the burner. This is primarily due to the inability to cool the surface down close to ambient temperature. The lowest surface temperature achieved was about 600 K. The model begins with species concentrations at their unburned, initial values; however, the experimental data shows significant consumption of initial species even at the first data point on the surface. For example, about half of the original unburned ethylene and oxygen is measured at the surface of the burner. Products such as carbon dioxide, carbon monoxide, and acetylene are also visible at the surface.

Reactions are beginning to take place before the surface of the burner because of the inability to adequately cool it.

Another observation is that the sharp features of the larger hydrocarbon species is not captured by the probe. This is most probably due to the probe taking a spatially averaged sample that is larger than its diameter (200 μm). The spatial averaging of the PREMIX data would serve to smooth out sharp features and better correlate to the experimental measurements.

The inability to cool the surface to atmospheric conditions and the spatial averaging of the probe should however play no role in the species measured far enough downstream where equilibrium is reached. For this reason, much of the focus should be placed on these equilibrium concentrations. The error of species concentrations expected at furthest distance from the surface is summarized in Table 2.
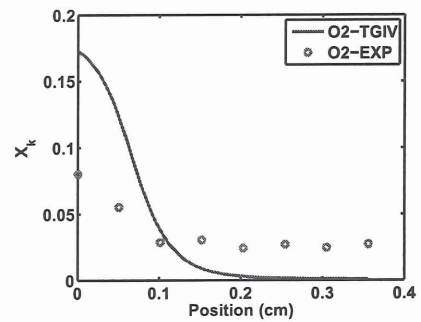
Table 2: Flat Flame Equilibrium Error

Species	Error
C_6H_6	85%
C_2H_2	26%
CH_4	5%
CO	12%
CO_2	12%
N_2	12%
H_2	1%

Due to the fact that a limited amount of data is available for this flat flame burner, it is difficult to accurately prescribe experimental uncertainty. A rough estimate of experimental deviation for this single round of data collection is done by taking a maximum and minimum window as a percentage of the experimental mean value of a previous iteration of the flat flame burner. This previous iteration of the burner largely maintained the same characteristics of the new burner, and thus much of the uncertainty from the experimental set up will be preserved. This deviation window as a percentage of the average species concentration is summarized in Table 3.

Table 3: Flat Flame Experimental Deviation

Species	Deviation
C_6H_6	63%
C_2H_2	28%
CH_4	26%
CO	26%
CO_2	28%
N_2	4%
H_2	21%

Overall, there is much better agreement in this data than that for the tube furnace. The extreme errors carbon dioxide and hydrogen found in the tube furnace are no longer present. Some species such as oxygen, however, were expected to be totally consumed downstream but were experimentally measured in significant quantities. Benzene and acetylene possessed the largest error of those species expected to be encountered by PREMIX. They also have the largest windows of deviation for the species of interest. It is important to note that benzene was never measured or expected in appreciable quantities in the tube furnace given its temperature limitations so comparison is unavailable. Benzene and acetylene are important compounds regarding soot formation and thus better agreement is desirable.
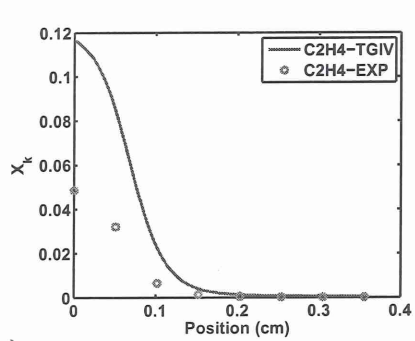
(a) C_2H_4
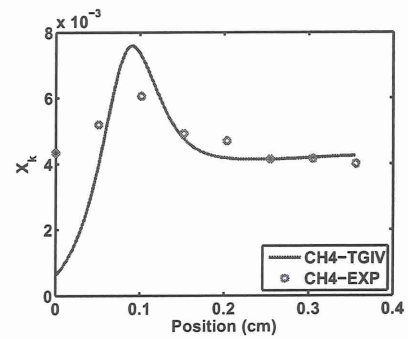
(b) CH_4
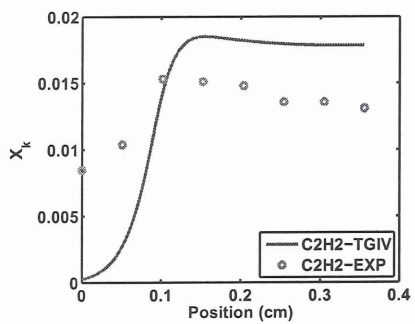
(c) C_2H_2

(d) O_2

(e) CO

(f) CO_2

(g) H_2

(h) N_2

(i) C_6H_6

(j) C_2H_6

(k) C_3H_6

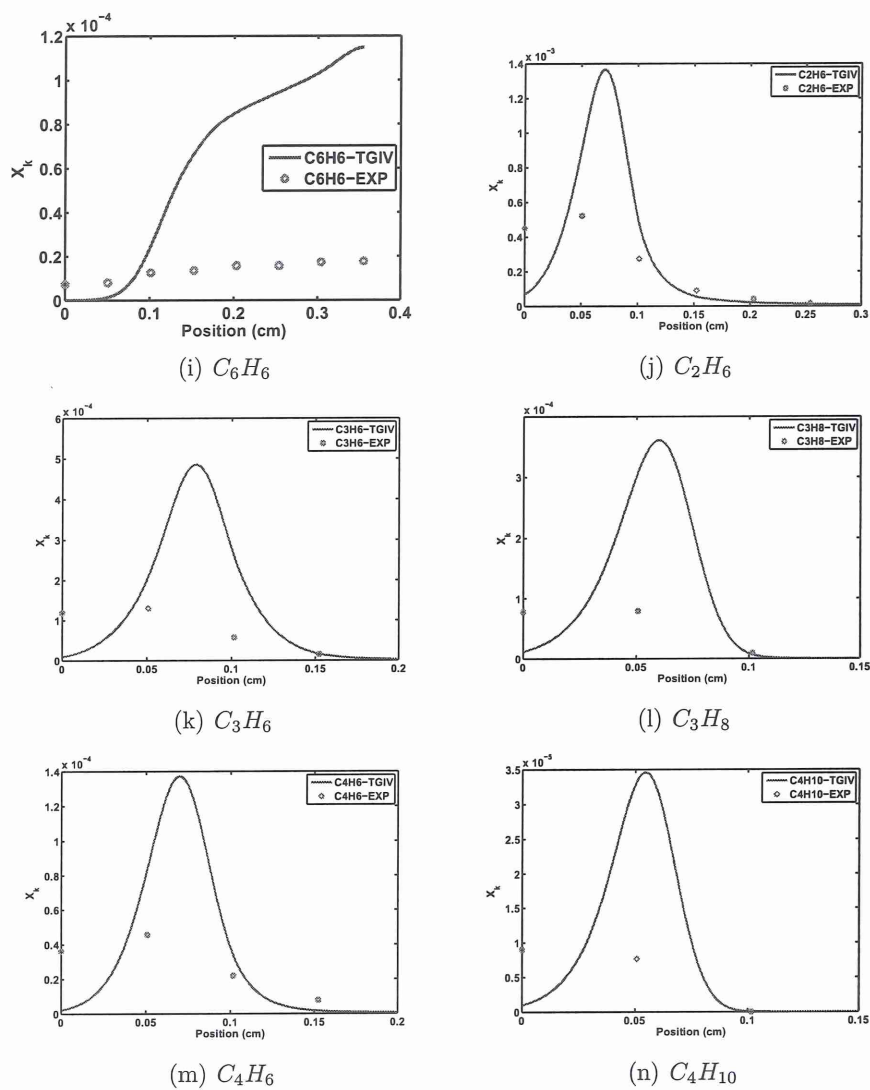(l) C_3H_8

(m) C_4H_6

(n) C_4H_{10}
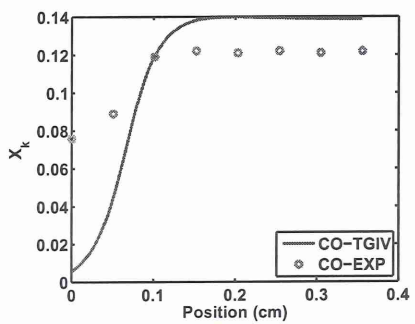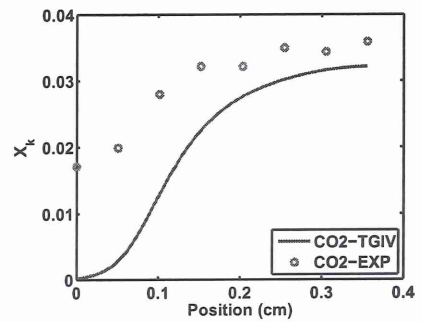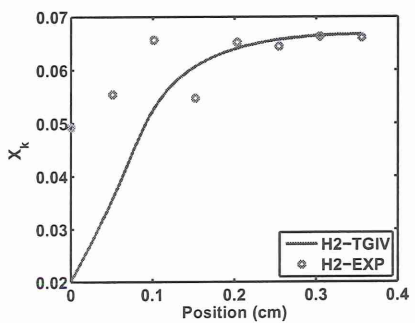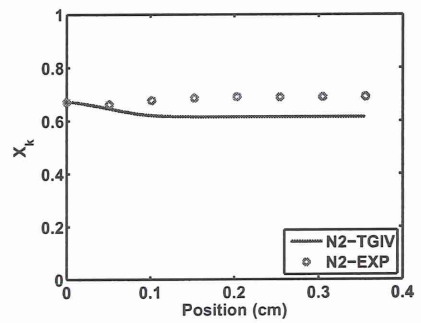
Figure 27: Experimental flat flame data and PREMIX model

6   Conclusion

A microflow tube reactor and a flat flame burner were used to analyze the formation of soot precursors, which are known to nucleate and grow into soot particles. Specifically, several reacting flow conditions were explored to test the applicability of a customized GC and GC/MS system for the conditions of interest.

Unfortunately, the current version of the tube reactor is unable to achieve all of the desired range of conditions as outlined in Section 3. Despite the inability to rapidly reach a target temperature for some extreme velocities and pressures, the reactor's experimental data can, for other conditions, be compared to that predicted using the reacting flow solver with detailed chemistry and transport models (PREMIX code). Under favorable experimental conditions, the measured species mole fractions at the reactor's outflow agreed reasonably well with those predicted from the PREMIX code. The PREMIX results for four of the eight measured species (C_2H_4, CH_4, O_2, N_2) fell within one standard deviation of the experimental data. Two of the other species (CO and C_2H_2) had errors of less 25% of the expected value from the PREMIX code, narrowly falling outside the standard deviation window. The last two species, CO_2 and H_2, had experimentally measured concentrations that differed significantly from modeled results.

Because of the differences in experimental and modeled species fractions found in the tube reactor, an alternate burner was developed for further comparison of the diagnosis method with the PREMIX code. This alternate burner is a "McKenna" style burner. This burner configuration has been extensively investigated and well characterized, so comparison with PREMIX code is beneficial for confirming the accuracy of the customized GC and GC/MS system. Overall, the experimental data for the flat flame burner agreed better than that of the tube reactor; however, less data was collected for the flat flame burner, giving its data less statistical significance. The experimental data for CO_2 and H_2 had much better agreement for the flat flame

burner compared to the tube reactor. Similar to the tube reactor, experimental data for CO and C_2H_2 in the flat flame burner was below the PREMIX code predictions. Benzene was experimentally measured only with the flat flame burner and this data differed drastically from the model.

Given the limitations of the current iteration of the tube reactor to generate soot precursor data for chemical model validation, some recommendations may improve future results. The block heaters used in the current iteration to rapidly increase fluid temperature are unsustainable at the high operating temperatures. The cartridge heating elements in the block heaters eventually lose the ability to maintain high temperatures over the course of their relatively short lifetime. Rapid heating of the fluid from the tube walls also introduces large radial temperature gradients that were shown to breakdown the plug flow assumption. Preheating the diluent and oxidizer and exploring improved methods of mixing of the fuel is perhaps more promising given the desirability of a flat, constant temperature at variable pressures and residence times. By not using clamped block heaters for heating, alternative tube materials such as quartz may be used in attempt to mitigate any catalytic effects of the inconel tube.

Once the chemical models that can predict soot precursors and soot are well validated, such models can be used in future CFD studies to optimize gas turbine and other combustion devices.

References

[1] D.J. Travis, A.M. Carleton, and R.G. Lauritsen. Climatology: Contrails reduce daily temperature range. *Nature*, 418(6898):601–601, 2002.

[2] D.J. Travis, A.M. Carleton, and R.G. Lauritsen. Regional variations in us diurnal temperature range for the 11-14 september 2001 aircraft groundings: evidence of jet contrail influence on climate. *Journal of climate*, 17(5):1123–1134, 2004.

[3] OB Popovicheva and AM Starik. Aircraft-generated soot aerosols: Physicochemical properties and effects of emission into the atmosphere. *Izvestiya Atmospheric and Oceanic Physics*, 43(2):125–141, 2007.

[4] ZA Mansurov. Soot formation in combustion processes (review). *Combustion, Explosion, and Shock Waves*, 41(6):727–744, 2005.

[5] H. Bennadji, PA Glaude, L. Coniglio, and F. Billaud. Experimental and kinetic modeling study of ethyl butanoate oxidation in a laminar tubular plug flow reactor. *Fuel*, 2011.

[6] MA Mueller, TJ Kim, RA Yetter, and FL Dryer. Flow reactor studies and kinetic modeling of the reaction h/o. *International Journal of Chemical Kinetics*, 1999.

[7] R.J. Kee, J.F. Grcar, MD Smooke, and JA Miller. Premix: a fortran program for modeling steady laminar one-dimensional premixed flames. *Sandia report SAND85-8240*, 1985.

[8] Holthuis & Associates. Mckenna flat flame burner, May 2012.

[9] B. G. Sarnacki, G. Esposito, R. H. Krauss, and H. K. Chelliah. Extinction limits and associate uncertainties of nonpremixed counterflow flames of methane, ethylene, propylene and n-butane in air. *Combustion and Flame*, 159(3):1026–1043, 2011.

[10] W.M. Pitts, E. Braun, R.D. Peacock, H.E. Mitler, EL Johnson, P.A. Reneke, and L.G. Blevins. Temperature uncertainties for bare-bead and aspirated thermocouple measurements in fire environments. *ASTM Special Technical Publication*, 1427:3–15, 2003.

[11] AG Worthing. Spectral emissivities of tantalum, platinum, nickel and gold as a function of temperature, and the melting point of tantalum. *Physical Review*, 28(1):174, 1926.

[12] S. Nakai and T. Okazaki. Heat transfer from a horizontal circular wire at small reynolds and grashof numbers. i-pure convection. ii-mixed convection. *International Journal of Heat and Mass Transfer*, 18:387–413, 1975.

[13] H.M. McNair, J.M. Miller, and MyiLibrary. *Basic gas chromatography*. Wiley Online Library, 1969.

[14] R.J. Ribando. *Heat transfer tools*. McGraw-Hill, 2002.

[15] E. Anderson, Z. Bai, C. Bischof, S. Blackford, J. Demmel, J. Dongarra, J. Du Croz, A. Greenbaum, S. Hammarling, A. McKenney, and D. Sorensen. *LAPACK Users' Guide*. Society for Industrial and Applied Mathematics, Philadelphia, PA, third edition, 1999.

[16] A. Bahadori. Prediction of compressed air transport properties at elevated pressures and high temperatures using simple method. *Applied Energy*, 88(4):1434–1440, 2011.

[17] A.F. Mills and AF Mills. *Basic heat and mass transfer*. Prentice hall Upper Saddle River, New Jersey, 1999.

[18] R.J. Kee, F.M. Rupley, E. Meeks, and J.A. Miller. *CHEMKIN-III: A FORTRAN*

chemical kinetics package for the analysis of gas-phase chemical and plasma kinetics. Sandia National Laboratories Livermore, CA, 1996.

[19] R.J. Kee and Sandia National Laboratories. *A Fortran computer code package for the evaluation of gas-phase, multicomponent transport properties.* Sandia National Laboratories, 1988.

[20] A.H. Shapiro. *Compressible Fluid Flow*, volume 1. 1953.

[21] B.R. Munson, D.F. Young, and T.H. Okiishi. *Fundamentals of fluid mechanics.* John Wiley & Sons, Inc., 1999.

A   Compressible Flow Analysis of Sampling Probe

Probing the gas sample at a back pressure of half an atmosphere motivated the compressible flow analysis described here. A MATLAB program was developed to predict the temperature, pressure, and velocity changes along the length of the probe as well as calculate the mass flow rate of sample to the GC and GC/MS. The required input parameters for the MATLAB program are:

- sample pressure that is probed (atm),

- length of probe (m),

- probe tip diameter (m),

- probe exit diameter (m),

- sample temperature (K),

- back pressure (atm).

The key assumptions made in the program include:

- steady flow,

- specific heat ratio $\gamma = 1.4$,

- tip of the probe is sonic, i.e. M = 1,

- shape of the probe is conical,

- frictionless, adiabatic flow through tip.

The program first calculates the sonic pressure (p^*) through the relation $\frac{p^*}{p_1} = 0.5283$. For the case where the sample is at atmospheric pressure, the sonic pressure will be greater than the back pressure and thus the system will choke. The code then uses an iterative algorithm where the area ratio of the shock location to the tip area is first

guessed and then solved through a bisection method. The first guess for this shock area ratio is the average of the minimum (1) and maximum ($\frac{A_{exit}}{A_{tip}}$) area ratios. The Mach number at the area associated with this ratio is calculated by [20]:

$$\frac{A}{A^*} = \frac{1}{M} \left[\left(\frac{2}{\gamma + 1} \right) \left(1 + \frac{\gamma - 1}{2} M^2 \right) \right]^{\frac{\gamma+1}{2(\gamma-1)}} . \tag{31}$$

Here, M is the upstream shock Mach number (M_x). The downstream shock Mach number (M_y) is then calculated from [21]:

$$M_y^2 = \frac{M_x^2 + \left[\frac{2}{\gamma-1} \right]}{\left[\frac{2\gamma}{\gamma-1} \right] M_x^2 - 1} . \tag{32}$$

The sonic area after the shock (A_y^*) is computed from equation (31) using this guessed shock area and M_y. Knowledge of the exit area of the probe allows for the determination of the Mach number at the exit of the probe (again by eq. (31)). The pressures at each side of the shock are calculated by [20]:

$$p_{0x} = p_x \left(1 + \frac{\gamma - 1}{2} M_x^2 \right)^{\frac{\gamma}{\gamma-1}} , \tag{33}$$

and [21]

$$\frac{p_y}{p_x} = \frac{1 + \gamma M_x^2}{1 + \gamma M_y^2} . \tag{34}$$

The stagnation pressure after the shock is then found from [21]:

$$\frac{p_{0y}}{p_{0x}} = \frac{\left(\frac{\gamma+1}{2} M_x^2 \right)^{\frac{\gamma}{\gamma-1}} \left(1 + \frac{\gamma-1}{2} M_x^2 \right)^{\frac{\gamma}{1-\gamma}}}{\left(\frac{2\gamma}{\gamma+1} M_x^2 - \frac{\gamma-1}{\gamma+1} \right)^{\frac{1}{\gamma-1}}} . \tag{35}$$

Finally, the pressure at the exit of the probe is calculated based on the guessed location of the shock [20]:

$$\frac{p_0}{p} = \left(1 + \frac{\gamma - 1}{2}M^2\right)^{\frac{\gamma}{\gamma-1}}. \tag{36}$$

If the guessed exit pressure is less than the back pressure, then the guessed shock occurred too late in the probe. The new guess for the area ratio of the shock will be smaller based on the bisection method. Alternatively, if the exit pressure of the guess is greater than the back pressure, then the shock occurred too soon and the bisection will guess a new larger area ratio. If the guessed exit pressure matches the back pressure then the iteration is complete. Now that the shock location is known, the Mach number, temperature, and pressure can be calculated at every point along the probe using equations (31), (36), and [20]:

$$\frac{T_0}{T} = 1 + \frac{\gamma - 1}{2}M^2. \tag{37}$$

The mass flow rate (kg/s) through the probe is found using [20]:

$$\frac{\dot{m}}{A^*} = \sqrt{\frac{\gamma}{R}\left(\frac{2}{\gamma+1}\right)^{\frac{\gamma+1}{\gamma-1}}} \frac{p_0}{\sqrt{T_0}}. \tag{38}$$

This is converted to standard liters per minute (SLPM) using the relation

$$\dot{V}_{SLPM} = \frac{\dot{m}}{(W/1000)} * 22.4 * 60. \tag{39}$$

For this report's experimental setup, the inputs for this code are:

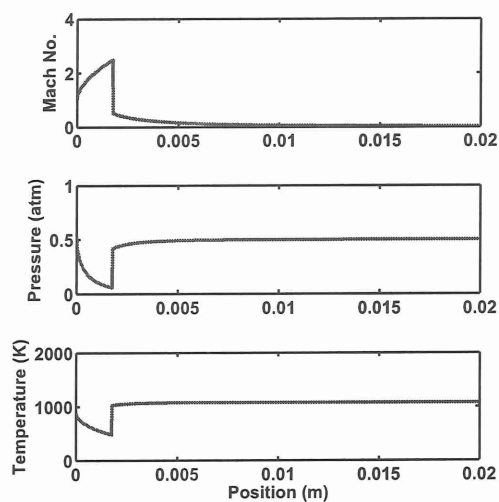- sample pressure probed = 1 atm,

- length of probe = 0.02 m ,

Figure 28: Mach no., pressure, and temperature along probe length

- probe tip diameter $= 200 * 10^{-6}$ m,

- probe exit diameter $= 1.6 * 10^{-3}$ m,

- sample temperature $= 900$ K,

- back Pressure $= 0.5$ atm.

The results are summarized in Figure 28. The shock occurs at a distance of 0.0018 m along the probe. The mass flow rates are:

$\dot{m} = 3.915 * 10^{-6}$ kg/s,

$\dot{V}_{SLPM} = 0.1816$ SLPM (air).

This mass flow rate in SLPM allows for the reasonable estimation of the pumping time necessary to completely flood the lines to the GC and GC/MS.